**Atmospheric
Chemistry
and Physics
Discussions**

Observationally-constrained estimates of global small-mode AOD

K. Lee and C. E. Chung

Dept. Environmental Science & Engineering, Gwangju Institute of Science and Technology, Gwangju, Korea

Correspondence to: C. E. Chung (eddy@gist.ac.kr)

ACPD

12, 31663–31698, 2012

Observationally-constrained estimates of global small-mode AOD

K. Lee and C. E. Chung

Title Page

Abstract	Introduction
Conclusions	References
Tables	Figures

|◄ | ►|

◄ | ►

Back | Close

Full Screen / Esc

Printer-friendly Version

Interactive Discussion

Full Screen / Esc

Printer-friendly Version

Interactive Discussion

Abstract

Small aerosols are mostly anthropogenic, and an area average of the small-mode aerosol optical depth (sAOD) is a powerful and independent measure of anthropogenic aerosol emission. We estimate AOD and sAOD globally on a monthly time scale from 2001 to 2010 by integrating satellite-based (MODIS and MISR) and ground-based (AERONET) observations. For sAOD, three integration methods were developed to maximize the influence of AERONET data and ensure consistency between MODIS, MISR and AERONET sAOD data. We evaluated each method by applying the technique with fewer AERONET data and comparing its output with the unused AERONET data. The best performing method gives an overall error of $13 \pm 2\%$, compared with an overall error of 62 % in simply using MISR sAOD, and this method takes advantage of an empirical relationship between the Ångström exponent (AE) and fine mode fraction (FMF). This relationship is obtained by analyzing AERONET data.

Using our integrated data, we find that the global 2001–2010 average of 500 nm AOD and sAOD is 0.17 and 0.094, respectively. sAOD over eastern China is several times as large as the global average. The linear trend from 2001 to 2010 is found to be slightly negative in global AOD or global sAOD. In India and eastern China combined, however, sAOD increased by more than 4 % against a backdrop of decreasing AOD and large-mode AOD. On the contrary to India and China, the west (Western Europe and US/Canada combined) is found to have a sAOD reduction of −20 %. These results quantify the overall anthropogenic aerosol emission reduction in the west, and rapidly deteriorating conditions in Asia. Moreover, our results in the west are consistent with the so-called surface brightening phenomenon in the recent decades.

1 Introduction

Solar radiation reaching the Earth's surface decreased in many regions of the world from the 1950's to the 1980's (e.g. Stanhill and Moreshet, 1992; Gilgen et al., 1998;

Stanhill and Cohen, 2001; Liepert, 2002), a phenomenon called "global dimming". Since then, a widespread increase in surface solar radiation has been observed, and this has been referred to as "global brightening" (Wild et al., 2005). One of the main causes of the global dimming and brightening is widely believed to be the change in the amount of atmospheric aerosols (Streets et al., 2009; Norris and Wild, 2009; Riihimaki et al., 2009).

Aerosols vary in time and space, and increasing aerosol amounts generally lower the downward surface solar radiation. Aerosols are emitted by anthropogenic sources as well as natural sources. Natural aerosols consist primarily of dust and sea salt particles, and these aerosols are mostly big in size. On the other hand, small aerosols in the submicron sizes are usually associated with black carbon, organic aerosol, sulfate, nitrate, etc., and these small particles are mostly anthropogenic. Anthropogenic aerosols tend to have lower single scattering albedo (SSA) values than natural aerosols (Chung et al., 2005), and lower SSAs have a higher efficiency in reducing the surface solar radiation (Chung, 2012). Therefore, if aerosol amount changes over time, it would be very important to partition the change between anthropogenic and natural ones, given the linkage to dimming and brightening phenomena.

The importance of small particles is amplified, when human health is an issue. Dockery et al. (1993) showed a strong relationship between mortality and air pollution with fine particulates, and Schwartz and Neas (2000) reported that small particles are more harmful for human respiratory health than coarse-sized particles.

This study is aimed at providing global and regional estimates of small-sized aerosol amounts. Such global estimates are already available in the form of aerosol optical depth (AOD; see Table 1 for the acronyms) and small-mode AOD derived from satellite measurements. More accurate estimates of sAOD are offered by ground-based aerosol networks such as the AErosol RObotic NETwork (AERONET; Holben et al., 1998). AERONET data have been widely used to validate satellite-derived data (Liu et al., 2004; Christopher and Wang, 2004; Martonchik et al., 2004; Kahn et al., 2005, 2010; Chu et al., 2002; Remer et al., 2002, 2005). On the other hand, because AERONET

Observationally-constrained estimates of global small-mode AOD

K. Lee and C. E. Chung

Title Page

Abstract	Introduction
Conclusions	References
Tables	Figures

◄ | ►|

◄ | ►

Back | Close

Full Screen / Esc

Printer-friendly Version

Interactive Discussion

Observationally-constrained estimates of global small-mode AOD

K. Lee and C. E. Chung

collects data from sparsely distributed stations, AERONET data is inadequate for global or regional mean estimates. The goal of the present study is to give global and regional mean sAOD (as well as AOD) estimates at the level of the AERONET data accuracy.

A global estimate of AOD at the AERONET data accuracy was made before by Chung et al. (2005) who integrated MODIS (Moderate Resolution Imaging Spectroradiometer) AOD and AERONET AOD. This study is significant expansion of Chung et al.'s (2005), in that (a) we bring in MISR (Multi-angle Imaging Spectroradiometer) data as well, (b) more importantly we address sAOD as well as AOD, and (c) we look at the trend of global and region mean AOD and sAOD. The trend of global and regional mean sAOD would be an independent and powerful measure of changes in global and regional anthropogenic aerosol emission. Typical air-quality monitoring such as PM (Particulate Matter) mass density measurement relies on unevenly-distributed sites, and so global or regional averages cannot be obtained reliably from these site measurements.

Aerosol data used in this study are described in Sect. 2. The techniques to integrate satellite and ground-based data for AOD and sAOD are discussed in Sects. 3 and 4, respectively. We discuss the trends of global and regional averages of AOD and sAOD in Sect. 5. Conclusion follows in Sect. 6.

2 Data

Table 2 summarizes the datasets used here. Below, we discuss the datasets in detail.

2.1 MODIS

The Moderate Resolution Imaging Spectroradiometer (MODIS) sensors onboard the Terra (launched in December 1999) and Aqua (launched in May 2002) satellites scan the atmosphere and the ocean surface in an unprecedented manner. The MODIS aerosol algorithm derives the ambient AOD over the oceans (Tanré et al., 2001) and

over the continents (Kaufman et al., 1997) on the globe. However, the MODIS data and algorithms are not adequate to retrieve AODs over bright surfaces such as deserts and snow surfaces (Kaufman et al., 1997). We downloaded the M3 product of Collection 5.1 data file, which is the latest monthly mean product. This product gives out AOD
5 and fine-mode fraction (FMF) which are then used to calculate sAOD.

AOD and sAOD data originally on the 1° by 1° spatial resolution are converted into the T42 resolution (approximately 2.8° by 2.8° grid) from 2001 to 2010, as follows. Over each T42 gridbox in each month, there are typically many values from the 1° × 1° Terra and Aqua data combined. If there are at least five values in a T42 gridbox, we use the
10 median to represent that T42 grid. Median, instead of arithmetic averaging, is a tool we choose in reducing cloud contamination. In a sensitivity test, we replace these median values by average values. We find that the global and decadal (2001–2010) mean AOD differs insignificantly between the two averaging methods. However, the 98th percentile AOD at 550 nm is about 50 % lower in the median method than in the average method.
15 This reduction is due mainly to removing many of extremely-large values in excess of 1.0. Monthly AOD exceeding 1.0 appears quite unrealistic and probably pertinent largely to cloud contamination, and thus eliminating many of these values should be viewed as improving the quality of AOD.

The Ångström exponent (AE) over the ocean is obtained using the T42-resolution
20 AOD at four wavelengths of 470, 550, 660 and 870 nm.

2.2 MISR

The Multi-angle Imaging Spectroradiometer (MISR) instrument aboard the Terra satellite (again, launched in December 1999) retrieves key aerosol optical properties, such as AOD, over the oceans and the continents including highly reflective surfaces like
25 deserts. We downloaded the CGAS MIL3MAE.004 product for the study. Out of this monthly product, we extracted AOD, sAOD, mAOD, lAOD and SSA. These parameters originally available on the 0.5° by 0.5° spatial resolution are converted into the T42 resolution using the median method that we adopted for the MODIS data processing in

Sect. 2.1. The effect of using the median method over the arithmetic averaging is assessed again, yielding similar results to that for MODIS AOD. The global and decadal (2001–2010) mean MISR AOD at 550 nm shows a small difference (about 0.01) between the median and arithmetic average methods. In case of the 98th percentile value,

5 AOD is about 40 % lower in the median method than in the average method.

Where necessary, we logarithmically interpolate AOD to the desired wavelength. We do the same logarithmical interpolation for other AOD data. MISR AE is computed using the T42-resolution AOD values at 443, 555, 670 and 865 nm.

2.3 AERONET

10 The AErosol RObotic NETwork (AERONET) is a ground-based aerosol network consisting of world-wide located automatic sun- and sky-scanning spectral radiometers (Holben et al., 1998). AERONET collects AOD from the direct sun measurements, and provides the retrieved optical parameters, such as SSA, using an inversion algorithm (Dubovik and King, 2000). sAOD and lAOD are computed from spectral AOD data us-

15 ing the spectral deconvolution algorithm of O'Neill et al. (2003). This algorithm assumes a bimodal aerosol size distribution.

We downloaded the monthly Level 2.0 (cloud-screened and quality-assured data) from AERONET Version 2 product, and the product includes the data from China. Among the various parameters of the dataset, we use AOD, sAOD and SSA fields.

20 AE is obtained using the AOD at three wavelengths of 440, 675 and 870 nm.

We calculate AOD and SSA at 550 nm, as follows. The 550 nm AOD is computed using logarithmic interpolation between AOD values at 500 nm and 675 nm. If AOD value is not available at 675 nm, values at 440 nm and 500 nm are extrapolated instead. If AOD value is not available at 500 nm, values at 440 nm and 675 nm are interpolated.

25 If AOD value is absent at two of these three wavelengths at least, AOD is not obtained at 550 nm. In case of SSA, the interpolation is done linearly between SSA values at 439 nm and 673 nm.

2.4 GOCART

The Georgia Tech/Goddard Global Ozone Chemistry Aerosol Radiation and Transport (GOCART) model simulates 550 nm AOD for major types of aerosols such as black carbon, organic carbon, sulfate, dust and sea salt (Chin et al., 2002). We use the GO-CART simulation as an interpolation tool to fill up the gaps in aerosol observations. The GOCART model produces a global gridded AOD at the 2.5° latitude by 2.0° longitude resolution, and the results are archived on a monthly scale from January 2000 to July 2002. All these products are interpolated onto the T42 resolution, and then averaged for each calendar month yielding climatological seasonal cycle.

GOCART SSA for total aerosols is computed using the AOD for each aerosol species, as in Chung et al. (2005), where SSAs of black carbon, organic carbon, sulfate, dust and sea salt are AOD-weighted averaged. Unlike in Chung et al. (2005), we use a black carbon SSA of 0.185 as theoretically obtained by Chung et al. (2012a), an organic carbon SSA of 0.85 as analyzed by Magi (2009), and a dust SSA of 0.96 as in Chung et al. (2012b). These new SSA values reflect recent advances in understanding the optical properties of aerosols.

The GOCART AOD is only available for 550 nm, and so we calculate AE using the AOD for each type of aerosols, as below:

$$
\text{GOCART\_AE} = \frac{1.65 \times \text{black carbon} + 1.7 \times \text{sulfate} + 1.31 \times \text{organic carbon} + 1.4 \times \text{sea salt} + 0.2 \times \text{dust}}{\text{Total AOD}(= \text{black carbon} + \text{sulfate} + \text{organic carbon} + \text{sea salt} + \text{dust})}
$$

(1)

In Eq. (1), "black carbon" refers to the GOCART-simulated black carbon AOD. In this equation, the values such as 1.65, 1.7, etc. represent typical AE values for each aerosol species and are obtained as follows. The dust AE of 0.2 is from Fig. 1a of Chung et al. (2012b). Figure 1a of Chung et al.'s (2012b) also shows that the biomass burning aerosol has an AE of 1.6. Given Magi's (2009, 2011) black carbon and organic carbon

Title Page

Abstract | Introduction

Conclusions | References

Tables | Figures

◄ | ►

Back | Close

Full Screen / Esc

Printer-friendly Version

Interactive Discussion

apportionment study, the biomass burning aerosol AE of 1.6 roughly translates into 1.65 for BC and 1.31 for organic carbon. The sulfate AE and sea slat AE are from Eq. (3) of Chung et al. (2005).

Please note that the GOCART AOD, SSA and AE are to fill up the observation gaps. Thus, the accuracy of these GOCART products is not a major concern in this study.

3 AOD, SSA, AAOD and AE integration

In this study, we integrate various aerosol datasets to produce the best estimates of AOD and sAOD. We also provide the best estimates of SSA and AAOD. In this section, we describe the integration procedures.

3.1 Aerosol optical depth (AOD)

First, we compare AERONET AODs with MODIS and MISR AODs in Fig. 2. Such comparison was made before (Chu et al., 2002; Remer et al., 2002, 2005; Kahn et al., 2005), revealing small differences between AERONET and MODIS/MISR data. The identified differences included generally negative biases by MODIS/MISR. Here we use monthly mean AODs for the comparison since the previous comparison was based on instantaneous AODs. The previously identified bias might be greater or smaller for monthly (mean) AOD for many reasons. For instance, AERONET, MODIS and MISR filter out data if deemed contaminated by cloud, and apply different filtering algorithms. This should result in differences in sampling clear and cloudy skies. A satellite study (Chand et al., 2009) showed a positive correlation between aerosol and cloud cover over the southern Atlantic Ocean, meaning that different sampling of clear and cloudy skies should contribute to monthly AOD bias while instantaneous AOD is irrelevant to these sampling differences. This compels that monthly AOD have different biases than instantaneous AOD. Validating monthly AOD has been done very little. Chung et al. (2005; hereafter referred to as Chung2005 for brevity) found larger differences

in monthly mean AOD between MODIS and AERONET than shown by instantaneous AOD investigation studies. In Chung2005, an older version of MODIS data was examined. In the present study, we use the latest version of MODIS AOD, and also include MISR data.

5   Here, we choose to validate monthly AODs at 550 nm as done in Chung2005. In the first step, MODIS and MISR AODs (before the T42 resolution conversion) are collocated in time and space with AERONET AODs. Any monthly AOD greater than 1.0 is considered cloud contaminated, and thus removed. Figure 2 displays the comparison of AERONET, MODIS and MISR AOD. As shown in Fig. 2, MODIS AOD (or MISR AOD)
10 is not well correlated with AERONET AOD. The correlation of about 0.7 ~ 0.8 is at the lower end of the 0.68 ~ 0.95 range (Chu et al., 2002; Remer et al., 2002, 2005; Kahn et al., 2005) identified for instantaneous AOD. MODIS data is in slightly better agreements with AERONET AOD than MISR data is (Fig. 2). The slopes in Fig. 2, on the other hand, correspond to the bias relative to AERONET AOD. The regression slopes
15 are found to be 0.61 for MISR (Fig. 2a) and 0.66 for MODIS (Fig. 2b), again in support of the superiority of MODIS AOD over MISR AOD. Previous instantaneous AOD studies reported that the regression slopes of MODIS on AERONET are 1.02 ± 0.05 for 660 nm AOD on a global scale (Remer et al., 2002), and 0.86 for 660 nm AOD over land (Chu et al., 2002). Remer et al. (2005) found the regression slope of 0.78 for 550 nm AOD
20 over land and 0.94 for 550 nm AOD over ocean. For instantaneous MISR AOD, Kahn et al. (2005) showed that the regression slopes of MISR versus AERONET AODs at 555 nm are 0.896 ± 0.003 for biomass burning aerosols, 0.681 ± 0.004 for continental aerosols, 0.693 ± 0.004 for dusty aerosols, and 1.381 ± 0.013 for maritime aerosols. By comparing our results with instantaneous AOD study results we conclude that monthly
25 AODs by MODIS/MISR tend to have greater biases than instantaneous AODs.

We also compare the global and decadal (2001–2010) mean of AERONET, MODIS, and MISR AOD with the global and 3 yr (2001–2003) means in Chung2005. The mean AOD values are 0.19 for AERONET, 0.18 for MODIS, and 0.17 for MISR here, while Chung2005 found the mean AERNET AOD to be 0.18 and the mean MODIS AOD to

be 0.26. The most salient difference between the results here and those of Chung2005 is that the difference between AERONET and MODIS AOD is sharply reduced here. Another noticeable difference is that MODIS and MISR now underestimate AODs compared to AERONET in contrast with the overestimated AOD by MODIS in Chung2005.

5 The differences between Chung2005's MODIS AOD and the MODIS AOD here are more than the period and the retrieval algorithm. In this study, we use median values in the conversion of MODIS and MISR data from the original resolution into the T42 resolution, and this median method significantly reduces the effect of cloud contamination while this sophisticated scheme was not adopted by Chung2005.

10 In view of the aforementioned errors of monthly MODIS/MISR AOD, it would be ideal to use AERONET AOD alone. Because AERONET collects data from sparsely distributed measurement sites over the globe, the AEROENT AOD gridded at the T42 resolution is dominated by gaps. To compensate for the data gaps, we combine the MODIS/MISR AOD with the AERONET AOD as in Chung2005. Chung2005 developed

15 a methodology of retaining the spatial patterns of MODIS AOD and adjusting them with the AERONET AOD values. We apply the overall approach of Chung2005, but deviate from Chung2005 in minor aspects.

We generate the combined AERONET + MODIS + MISR 550-nm AOD as follows. The data combination is conducted for each month from 2001 to 2010. We use GO-

20 CART simulations to fill the gaps in MISR or MODIS AOD. The MISR, MODIS, and AERONET AODs are assimilated so that the order of influence is AERONET > MODIS > MISR > GOCART. MODIS seems to be more accurate than MISR in view of Fig. 2, and this is the basis for designing greater influence of MODIS than of MISR AOD. The assimilation takes place in three steps: (i) The MISR AOD bias of 0.0286, com-

25 pared to the AERONET AOD, is added to the MISR AOD at each grid. This bias is the global and decadal average of the difference between collocated AERONET and MISR AODs. We then fill the gaps of these MISR AODs with GOCART AODs using the interative difference-successive correction method developed by Cressman (1959). (ii) The MODIS AOD bias of 0.0110 is added to the MODIS AOD at each grid. Then, the gaps

Title Page

Abstract | Introduction

Conclusions | References

Tables | Figures

◄ | ►

◄ | ►

Back | Close

Full Screen / Esc

Printer-friendly Version

Interactive Discussion

in the MODIS AODs are filled with the MISR + GOCART AOD again using Cressman's (1959) approach. (iii) The spatial pattern in the MODIS + MISR + GOCART AOD is coupled with the sparsely distributed AERONET AOD values, using Chung2005's technique, as below.

$$N_{\text{AOD}}j = \text{MMG}_{\text{AOD}}j \times \frac{\sum_i \frac{\text{AERONET}_{j,i}}{d_{j,i}^{4}}}{\sum_i \frac{\text{MMG}_{\text{AOD}}j,i}{d_{j,i}^{4}}} \qquad (2)$$

where $N_{\text{AOD}}j$ is the adjusted new value of the AOD at grid j; $\text{AERONET}_{j,i}$ is an AERONET AOD at station location i nearby grid j; $d_{j,i}$ is the distance between j and i; and $\text{MMG}_{\text{AOD}}j,i$ is the MODIS + MISR + GOCART AOD at the grid of $\text{AERONET}_{j,i}$. Final AOD (i.e. N_{AOD}) matches AERONET AOD wherever AERONET AOD exists.

Figure 3a shows the 2001–2010 mean of the integrated AOD. AOD is large over eastern China, the middle Africa and India, as expected. There is a lot of biomass burning over the middle Africa while fossil fuel combustion has been increasing significantly in India and China. The global and decadal (2001–2010) mean is 0.16.

3.2 Single scattering albedo (SSA)

We generate global SSA only with GOCART SSA and AERONET SSA. MODIS does not provide SSA data and the SSA from MISR appears to be quite unrealistic. GOCART SSA is for 550 nm, and is subsequently adjusted by 550 nm AERONET SSA as in Chung2005. The final SSA is for each month from 2001 to 2010, and the decadal average is shown in Fig. 3b. In computing the decadal average SSA, the averaging is AOD weighted. The lowest SSA, which points to very absorbing aerosols, is found over the biomass burning areas in Africa. Areas with heavy industry such as eastern China do not show low SSA, probably because scattering anthropogenic aerosols such as sulfate are plentiful over there.

31673

3.3 Absorption aerosol optical depth (AAOD)

We obtain AAOD using the integrated AOD and SSA at 550 nm. The relationship between AOD, AAOD and SSA is given by Eq. (3).

$$AAOD(\lambda) = AOD(\lambda) \times [1 - SSA(\lambda)] \tag{3}$$

Figure 3c displays the 10-yr (2001–2010) average of this AAOD. AAOD is very large over eastern China and the middle Africa.

3.4 Ångström exponent for AOD (AE)

As we integrate various datasets for AOD, we combine MODIS, MISR, AERONET and GOCART AEs for our best estimate of AE, except that we combine MODIS and MISR data as follows. We only use the MODIS AE over the ocean and use the MISR AE over the land. We choose to do this, because the MODIS AOD over the land is only available at three wavelengths of 470, 550 and 660 nm while over the ocean the AOD is additionally offered at 870 nm. Because we will adjust the MODIS AE with the AERONET AE and the AERONET AE is computed using the AOD over 440–870 nm, we only use the MODIS AOD over the ocean to compute the MODIS AE for consistency. Figure 4b shows the MODIS AE; in this figure the land AE is computed using the AODs at 470, 550 and 660 nm. As shown in Fig. 4b, there is clear discontuity between the MODIS AE over the land and the AE over the ocean. The MISR AE (Fig. 4a) on the other hand does not suffer the discontuity.

Our best AE estimate, which integrates AERONET, MODIS and MISR data, is shown in Fig. 4c. The overall pattern does not show the aforementioned discontuity, and is very consistent with the spatial distribution of average particle size. AE is inversely proportional to particle size, and should be small over the ocean and deserts where aerosols are generally large. As shown in Fig. 4c, large AE values are dominant over the biomass burning areas and industrial regions.

Title Page

Abstract | Introduction

Conclusions | References

Tables | Figures

|◄ | ►|

◄ | ►

Back | Close

Full Screen / Esc

Printer-friendly Version

Interactive Discussion

4 Small-mode aerosol optical depth (sAOD) integration

For our best estimates of sAOD, we integrate AERONET, MODIS and MISR data and GOCART simulation as we did for AOD. Applying the exactly same integration method will not work, because AERONET, MODIS and MISR use different particle cut-off sizes to define sAOD (see Table 3). For example, MODIS sAOD represents smaller particles than AERONET sAOD does, and thus MODIS sAOD would have a low bias relative to AERONET sAOD. To overcome this problem, we design two methods. In addition, the simple integration method that was used for AOD is applied for the comparison. In the following subsections, we discuss and evaluate the three methods.

4.1 Method 1: using AE

The overall strategy of the first method is to use AE to derive sAOD. AE was computed using AODs, and MODIS, MISR and AERONET AODs do not have the bias issue that sAODs have. AE is known to give information about aerosol size (King et al., 1978; Nakajima et al., 1986; Kaufman, 1993; Eck et al., 1999; O'Neill et al., 2001a, b, 2003; Schuster et al., 2006). Thus, it is conceivable that AE is related to sAOD, and yet the relationship between the two has not been investigated to our knowledge. Here, we attempt to investigate this relationship, but a direct comparison does not work well since sAOD is proportional to aerosol amount while AE is not. Therefore, to better quantify the relationship between sAOD and AE, we replace sAOD by FMF (the fine-mode fraction) which is the ratio of sAOD to AOD.

We analyze the relationship between AE and 500 nm FMF, using monthly AERONET data, as shown in Fig. 5. AE is correlated remarkably well with FMF! We find that this positive relationship is also reproduced by running a Mie scattering code. We use a Mie scattering code to produce additional AE/FMF data when AE > 2.0, since there are so few data with AE > 2.0 in Fig. 5. Then, we divide Fig. 5 into two regions to find the most realistic best-fit line in each region. The best-fit equations are shown in Fig. 5.

The sAOD estimate is obtained, as follows. (i) These fitting equations are applied to compute global FMF using the integrated AE. (ii) The obtained FMF is multiplied by the integrated AOD to compute sAOD. (iii) This sAOD is adjusted by AERONET sAOD, using Eq. (2). These 3 steps constitute the first method.

Figure 6a depicts the sAOD obtained in this fashion. The most noticeable feature in Fig. 6a is that sAOD is largest over eastern China. Compared to total AOD in Fig. 3a, sAOD is particularly large in China. This contrast between AOD and sAOD is in our view the most unexpected aspect of our obtained sAOD. Based on this, we propose that small (in size) aerosols are a major component of aerosols in eastern China. As will be shown later, this method is our best method, and gives more accurate data than MODIS or MISR data alone.

Our finding that aerosols in China are mostly made up of small particles cannot be reached using an AERONET data analysis alone, since there are so few AERONET stations in China. On the other hand, MISR and MODIS give a global picture of sAOD. In Fig. 6 we compare the integrated sAOD (Fig. 6a) with MISR sAOD (Fig. 6b) and MODIS sAOD (Fig. 6c) In MISR or MODIS data, sAOD is not particularly large over eastern China. Furthermore, the MODIS sAOD is not available over much of the land.

4.2 Method 2: FMF integration

The second method is based exclusively on FMF. The concept of the method is that differing definitions of sAOD create biases in FMF and we compute these biases for the correction.

First, we compare AERONET FMF with MODIS/MISR FMF. Here, we define MISR FMF as the ratio of sAOD + mAOD to tAOD, since MISR sAOD + mAOD explains a range of particle size similar to that of AERONET/MODIS sAOD (see Table 3). When monthly AERONET data are compared to MODIS or MISR data after collocation in time and space, we find that MISR FMF is better correlated with AERONET FMF than MODIS. In view of this, we allow greater influence of MISR FMF than MODIS FMF.

The second method is conducted in five steps: (i) Collocated AERONET and MODIS AOD and sAOD from 2001 to 2010 are globally averaged, showing that the AERONET FMF is 40 % larger than the MODIS FMF on the average. We multiply the MODIS FMF at each grid point by 1.4 (i.e. 140 %) to bring it on a par with the AERONET FMF. We then fill the gaps of this adjusted MODIS FMFs with GOCART FMFs using Cressman's (1959) method. (ii) The gaps in MISR FMFs are filled with the MODIS + GOCART FMFs using again Cressman's (1959) approach. The MISR FMF is multiplied by 0.98 at each grid to be on a par with the AERONET FMF. (iii) The spatial pattern in the MISR + MODIS + GOCART FMF is coupled with the sparsely distributed AERONET FMFs, using Eq. (2). (iv) The combined AERONET + MISR + MODIS + GOCART FMF is multiplied by our best AOD estimate to obtain sAOD. (v) This sAOD is adjusted by AERONET sAOD again using Eq. (2).

4.3 Method 3: simple sAOD integration

In this method, we integrate MODIS, MISR and AERONET sAODs without regard to the different sAOD definitions, using the exactly same integration method as for AOD. This method needs to be implemented, in order to quantify the performance of the previous methods. Like AOD, we find that MODIS sAOD is better correlated with AERONET sAOD than MISR sAOD.

The integration takes place as follows: (i) The MISR sAOD + mAOD bias of 0.015412, compared to the AERONET sAOD, is added to the MISR sAOD + mAOD at each grid. This bias is the global and decadal average of the difference between collocated AERONET sAOD and MISR sAOD + mAOD. We then fill the gaps of these MISR sAOD + mAOD with GOCART sAOD (sum of AODs for black carbon, organic carbon, and sulfate) using Cressman's (1959) method. (ii) The MODIS sAOD bias of 0.051476 is added to the MODIS sAOD at each grid. Then, the gaps in the MODIS sAOD are filled with the MISR + GOCART sAOD again using Cressman's (1959) approach. (iii) The spatial pattern in the MODIS + MISR + GOCART sAOD is coupled with the sparsely distributed AERONET sAOD using Eq. (2).

Full Screen / Esc

Printer-friendly Version

Interactive Discussion

4.4 Evaluating the three methods

We evaluate the three methods by applying each method with fewer AERONET data and then comparing the estimated sAOD with the unused AERONET sAOD data. This evaluation process is repeated with (randomly-chosen) different choices of the unused AERONET data. These different choices are spatially as well as temporally based. The errors are then averaged in space and time and also over the difference choices of the unused data.

We find that the best performing method is the first method which is AE based. An overall error for the first method is $13 \pm 2\%$, and this is significant improvement over the simple use of MISR sAOD which gives an overall error of 62 %. ±2 % represents the uncertainty due to sampling the unused AERONET data. The second and third methods yield an overall error of $31 \pm 3\%$ and $89 \pm 18\%$, respectively.

5 Linear trend in AOD and sAOD

Figure 7 displays the time series of area-averaged annual-mean AOD and sAOD from 2001 to 2010. The AOD and sAOD in Figs. 7 and 8 are from our best estimates. Focusing on the global average, AOD and sAOD were on the increase till 2005 and then on the decrease afterwards. There are a short-term sAOD reduction in 2006 and another reduction in 2008. The year-2006 reduction comes significantly from South America, which is known to emit a lot of biomass smoke. In the 2008 reduction, Southeast Asia as well as South America played an important role. As Fig. 7b shows, sAOD was down a lot in 2008 due partly to Western Europe. Because fossil fuel combustion is the dominant anthropogenic emission source in this region (Lamarque et al., 2010), this short-term sAOD reduction in Western Europe might have been associated with the economic recession in 2008. Recession is accompanied by less consumption, less transportation and smaller industrial output, which are expected to drive down sulfate concentration. On the other hand, biomass burning, the source of which includes wild

forest fire and indoor wood combustion, can be regarded as less dependent on overall economy.

Turning to regional averages, AOD and sAOD tended to decrease over the 10 yr in US/Canada sector, Western Europe sector and Eastern Europe/Soviet Union sector (Fig. 7). For Western Europe and US/Canada combined, AOD and sAOD were down 20 % in the decade (Table 4a). However, sAOD had a strong increase in China and India sectors. In India and eastern China collectively, AOD decreased slightly while sAOD was up 43 %. sAOD could only increase against a backdrop of decreasing AOD, if large-mode AOD decreases significantly. If large-mode AOD, which mostly represents natural aerosols, did not change in this sector of the world, the level of PM would have gone up huge in this region.

Using AERONET data alone (Table 4b), sAOD was only up 16 % in India and eastern China combined. There are an insufficient number of AERONET sites in this region to properly represent the region, and the difference between Table 4a and b corroborates this. The area-average sAOD estimates are the novelty of the present study.

The decreasing tendency in AOD and sAOD in the west (from Fig. 7 and Table 4a) is consistent with PM observation studies. For example, Wang et al. (2011) showed a decreasing trend in $PM_{2.5}$ concentration in New York from 2002 to 2009, and Wåhlin (2009) reported that the average particle number concentration at the kerbside of a busy street in Copenhagen had gone down 27 % from the period 2002–2004 to the period 2005–2007.

Table 4a also shows that while sAOD increased in India and eastern China combined, AAOD decreased. Not all the aerosol species absorb solar radiation, and the primary absorbing species are dust, black carbon and organic carbon (Chung et al., 2012b). Since large-mode AOD was down significantly in this region, a very large reduction in dust amount is likely a major explanation for the AAOD reduction. A reduction in carbonaceous aerosols is not a good explanation for the AAOD decrease because such a reduction is not supportive of the sAOD increase.

Title Page

Abstract | Introduction

Conclusions | References

Tables | Figures

|◄ | ►|

◄ | ►

Back | Close

Full Screen / Esc

Printer-friendly Version

Interactive Discussion

A global pattern of the linear trend in AOD and sAOD is displayed in Fig. 8. sAOD increases are only pronounced over India and eastern China. The reduction in AOD or sAOD is widespread in the west. These results are consistent with the identified dimming and brightening in various regions around the world. Wild et al. (2009) showed a brightening phenomenon for the period from 2000 to 2005 in Europe and USA, and a dimming phenomenon in India and China/Mongolia. Long et al. (2009) also reported a widespread brightening for 12 yr (1995–2007) over the continental United State.

6 Discussion

Through this study, we have sought to provide the best estimates of global AOD, sAOD and AAOD by integrating various aerosol observations. Our estimates have a variety of uses. In one use, our product can be used to validate aerosol simulations. Satellite-based AODs have been commonly used for such validation (e.g. Kinne et al., 2006) and in some cases (e.g. Myhre et al., 2009) AERONET AODs were used. The AOD we have offered here is global and should be considered more accurate than pure satellite-based values, and moreover we have also offered global sAOD. In another use, the ratio of sAOD to AOD can be used to roughly determine the anthropogenic fraction of total aerosol. In the previous aerosol forcing estimation studies (e.g. Chung et al., 2005; Bellouin et al., 2005, 2008), the anthropogenic fraction was derived entirely or partially from aerosol simulations. Our global sAOD product can make it possible to derive the anthropogenic fraction without using a model.

In this study, we have also demonstrated the usefulness of our product by analyzing the area averages of sAOD. The principal findings of the present study are from the sAOD area averages. sAOD area averages are a powerful and independent measure of anthropogenic aerosol emission. A sAOD area average by itself does not provide the amount of emission, but the time series of sAOD area averages can be used to quantify the trend of anthropogenic aerosol emission. Aerosol emission inventory studies (e.g. Lamarque et al., 2010; Smith et al., 2011) are subject to a lot of error sources and

Title Page

Abstract | Introduction

Conclusions | References

Tables | Figures

⏮ | ⏭

◀ | ▶

Back | Close

Full Screen / Esc

Printer-friendly Version

Interactive Discussion

uncertainties. For black carbon emission alone, there is a factor of 2 or more uncertainty in the estimates (Bond et al., 2004, 2007). Given these uncertainties, the time series of our sAOD area averages is particularly valuable.

Lastly, the time series of our AOD and sAOD area averages quantifies the overall trend of aerosols. Direct measurement of aerosol concentrations in the ambient atmosphere is station or site based, and cannot be used to monitor overall air quality over a large area.

References

Bellouin, N., Boucher, O., Haywood, J., and Reddy, M. S.: Global estimate of aerosol direct radiative forcing from satellite measurements, Nature, 438, 1138–1141, doi:10.1038/nature04348, 2005.

Bellouin, N., Jones, A., Haywood, J., and Christopher, S. A.: Updated estimate of aerosol direct Radiative forcing from satellite observations and comparison against the centre climate model, J. Geophys. Res., 113, D10205, doi:10.1029/2007JD009385, 2008.

Bond, T. C., Streets, D. G., Yarber, K. F., Nelson, S. M., Woo, J.-H., and Klimont, Z.: A technology-based global inventory of black and organic carbon emissions from combustion, J. Geophys. Res., 109, D14203, doi:10.1029/2003JD003697, 2004.

Bond, T. C., Bhardwaj, E., Dong, R., Jogani, R., Jung, S., Roden, C., Streets, D. G., and Trautmann, N. M.: Historical emissions of black and organic carbon aerosol from energy-related combustion, 1850–2000, Global Biogeochem. Cy., 21, GB2018, doi:10.1029/2006GB002840, 2007.

Chand, D., Wood, R., Anderson, T. L., Satheesh, S. K., and Charlson, R. J.: Satellite-derived direct radiative effect of aerosols dependent on cloud cover, Nat. Geosci., 2, 181–184, doi:10.1038/NGEO437, 2009.

Chin, M., Ginoux, P., Kinne, S., Torres, O., Holben, B. N., Duncan, B. N., Martin, R. V., Logan, J. A., Higurashi, A., and Nakajima, T.: Tropospheric aerosol optical thickness from the

Observationally-constrained estimates of global small-mode AOD

K. Lee and C. E. Chung

Title Page

Abstract	Introduction
Conclusions	References
Tables	Figures

◀ | ▶

◀ | ▶

Back | Close

Full Screen / Esc

Printer-friendly Version

Interactive Discussion

GOCART model and comparisons with satellite and sun photometer measurements, J. Atmos. Sci., 59, 461–483, 2002.

Christopher, S. A. and Wang, J.: Intercomparison between multi-angle imaging spectroradiometer (MISR) and sunphotometer aerosol optical thickness in dust source regions over China: implications for satellite aerosol retrievals and radiative forcing calculations, Tellus B, 56, 451–456, 2004.

Chu, D. A., Kaufman, Y. J., Ichoku, C., Remer, L. A., Tanré, D., and Holben, B. N.: Validation of MODIS aerosol optical depth retrieval over land, Geophys. Res. Lett., 29, 1617, doi:10.1029/2001GL013205, 2002.

Chung, C. E.: Aerosol direct radiative forcing: a review, in: Atmospheric Aerosols – Regional Characteristics – Chemistry and Physics, edited by: Hayder Abdul-Razzak, ISBN: 978-953-51-0728-6, InTech, available at: http://www.intechopen.com/books/atmospheric-aerosols-regional-characteristics-chemistry-and-physics/aerosol-direct-radiative-forcing-a-review, 2012.

Chung, C. E., Ramanathan, V., Kim, D., and Podgorny, I. A.: Global anthropogenic aerosol direct forcing derived from satellite and ground-based observations, J. Geophys. Res., 110, D24207, doi:10.1029/2005JD006356, 2005.

Chung, C. E., Lee, K., and Müller, D.: Effect of internal mixture on black carbon radiative forcing, Tellus B, 64, doi:10.3402/tellusb.v64i0.10925, 2012a.

Chung, C. E., Ramanathan, V., and Decremer, D.: Observationally constrained estimates of carbonaceous aerosol radiative forcing, P. Natl. Acad. Sci., 109, 11624–11629, 2012b.

Cressman, G. P.: An operational objective analysis system, Mon. Weather Rev., 87, 367–374, 1959.

Dockery, D. W., Pope, C. A., Xu, X., Spengler, J. D., Ware, J. H., Fay, M. E., Ferris, B. G., and Speizer, F. E.: An association between air pollution and mortality in six US cities, New Engl. J. Med., 329, 1753–1759, doi:10.1056/NEJM199312093292401, 1993.

Dubovik, O. and King, M. D.: A flexible inversion algorithm for retrieval of aerosol optical properties from Sun and sky radiance measurements, J. Geophys. Res., 105, 20673–20696, 2000.

Eck, T. F., Holben, B. N., Reid, J. S., Dubovik, O., Smirnov, A., O'Neill, N. T., Slutsker, I., and Kinne, S.: Wavelength dependence of the optical depth of biomass burning, urban, and desert dust aerosols, J. Geophys. Res., 104, 31333–31349, doi:10.1029/1999JD900923, 1999.

Title Page

Abstract | Introduction

Conclusions | References

Tables | Figures

◄ | ►

◄ | ►

Back | Close

Full Screen / Esc

Printer-friendly Version

Interactive Discussion

Gilgen, H., Wild, M., and Ohmura, A.: Means and trends of shortwave irradiance at the surface estimated from global energy balance archive data, J. Climate, 11, 2042–2061, 1998.

Holben, B. N., Eck, T. F., Slutsker, I., Tanré, D., Buis, J. P., Setzer, A., Vermote, E., Reagan, J. A., Kaufman, Y. J., Nakajima, T., Lavenu, F., Jankowiak, I., and Smirnov, A.: AERONET – a federated instrument network and data archive for aerosol characterization, Remote Sens. Environ., 66, 1–16, 1998.

Kahn, R. A., Gaitley, B. J., Martonchik, J. V., Diner, D. J., Crean, K. A., and Holben, B.: Multiangle Imaging Spectroradiometer (MISR) global aerosol optical depth validation based on 2 years of coincident Aerosol Robotic Network (AERONET) observations, J. Geophys. Res., 110, D10S04, doi:10.1029/2004JD004706, 2005.

Kahn, R. A., Gaitley, B. J., Garay, M. J., Diner, D. J., Eck, T. F., Smirnov, A., and Holben, B. N.: Multiangle Imaging SpectroRadiometer global aerosol product assessment by comparison with the Aerosol Robotic Network, J. Geophys. Res., 115, D23209, doi:10.1029/2010JD014601, 2010.

Kaufman, Y. J.: Aerosol optical thickness and atmospheric path radiance, J. Geophys. Res., 98, 2677–2692, doi:10.1029/92JD02427, 1993.

Kaufman, Y. J., Tanré, D., Remer, L. A., Vermote, E. F., Chu, A., and Holben, B. N.: Operational remote sensing of tropospheric aerosol over land from EOS moderate resolution imaging spectroradiometer, J. Geophys. Res., 102, 17051–17067, doi:10.1029/96JD03988, 1997.

King, M. D., Byrne, D. M., Herman, B. M., and Reagan, J. A.: Aerosol size distributions obtained by inversions of spectral optical depth measurements, J. Atmos. Sci., 35, 2153–2167, 1978.

Kinne, S., Schulz, M., Textor, C., Guibert, S., Balkanski, Y., Bauer, S. E., Berntsen, T., Berglen, T. F., Boucher, O., Chin, M., Collins, W., Dentener, F., Diehl, T., Easter, R., Feichter, J., Fillmore, D., Ghan, S., Ginoux, P., Gong, S., Grini, A., Hendricks, J., Herzog, M., Horowitz, L., Isaksen, I., Iversen, T., Kirkevåg, A., Kloster, S., Koch, D., Kristjansson, J. E., Krol, M., Lauer, A., Lamarque, J. F., Lesins, G., Liu, X., Lohmann, U., Montanaro, V., Myhre, G., Penner, J., Pitari, G., Reddy, S., Seland, O., Stier, P., Takemura, T., and Tie, X.: An AeroCom initial assessment – optical properties in aerosol component modules of global models, Atmos. Chem. Phys., 6, 1815–1834, doi:10.5194/acp-6-1815-2006, 2006.

Lamarque, J. F., Bond, T. C., Eyring, V., Granier, C., Heil, A., Klimont, Z., Lee, D., Liousse, C., Mieville, A., Owen, B., Schultz, M. G., Shindell, D., Smith, S. J., Stehfest, E., Van Aardenne, J., Cooper, O. R., Kainuma, M., Mahowald, N., McConnell, J. R., Naik, V., Riahi, K., and van Vuuren, D. P.: Historical (1850–2000) gridded anthropogenic and biomass burning

emissions of reactive gases and aerosols: methodology and application, Atmos. Chem. Phys., 10, 7017–7039, doi:10.5194/acp-10-7017-2010, 2010.

Liepert, B. G.: Observed reductions of surface solar radiation at sites in the United States and worldwide from 1961 to 1990, Geophys. Res. Lett., 29, 1421, doi:10.1029/2002GL014910, 2002.

Liu, Y., Sarnat, J. A., Coull, B. A., Koutrakis, P., and Jacob, D. J.: Validation of Multiangle Imaging Spectroradiometer (MISR) aerosol optical thickness measurements using Aerosol Robotic Network (AERONET) observations over the contiguous United States, J. Geophys. Res., 109, D06205, doi:10.1029/2003JD003981, 2004.

Long, C. N., Dutton, E. G., Augustine, J. A., Wiscombe, W., Wild, M., McFarlane, S. A., and Flynn, C. J.: Significant decadal brightening of downwelling shortwave in the continental United States, J. Geophys. Res., 114, D00D06, doi:10.1029/2008JD011263, 2009.

Magi, B. I.: Chemical apportionment of southern African aerosol mass and optical depth, Atmos. Chem. Phys., 9, 7643–7655, doi:10.5194/acp-9-7643-2009, 2009.

Magi, B. I.: Corrigendum to "Chemical apportionment of southern African aerosol mass and optical depth" published in Atmos. Chem. Phys., 9, 7643–7655, 2009, Atmos. Chem. Phys., 11, 4777–4778, doi:10.5194/acp-11-4777-2011, 2011.

Martonchik, J. V., Diner, D. J., Kahn, R., Gaitley, B., and Holben, B. N.: Comparison of MISR and AERONET aerosol optical depths over desert sites, Geophys. Res. Lett., 31, L16102, doi:10.1029/2004GL019807, 2004.

Myhre, G., Berglen, T. F., Johnsrud, M., Hoyle, C. R., Berntsen, T. K., Christopher, S. A., Fahey, D. W., Isaksen, I. S. A., Jones, T. A., Kahn, R. A., Loeb, N., Quinn, P., Remer, L., Schwarz, J. P., and Yttri, K. E.: Modelled radiative forcing of the direct aerosol effect with multi-observation evaluation, Atmos. Chem. Phys., 9, 1365–1392, doi:10.5194/acp-9-1365-2009, 2009.

Nakajima, T., Takamura, T., Yamano, M., Shiobara, M., Yamauchi, T., Goto, R., and Murai, K.: Consistency of aerosol size distributions inferred from measurements of solar radiation and aerosols, J. Met. Soc. Jap., 64, 765–776, 1986.

Norris, J. R. and Wild, M.: Trends in aerosol radiative effects over China and Japan inferred from observed cloud cover, solar "dimming", and sola "brightening", J. Geophys. Res., 114, D00D15, doi:10.1029/2008JD011378, 2009.

Printer-friendly Version

Interactive Discussion

O'Neill, N. T., Eck, T. F., Holben, B. N., Smirnov, A., Dubovik, O., and Royer, A.: Bimodal size distribution influences on the variation of Angstrom derivatives in spectral and optical depth space, J. Geophys. Res., 106, 9787–9806, 2001a.

O'Neill, N. T., Dubovik, O., and Eck, T. F.: Modified Ångström exponent for the characterization of submicrometer aerosols, Appl. Opt., 40, 2368–2375, 2001b.

O'Neill, N. T., Eck, T. F., Smirnov, A., Holben, B. N., and Thulasiraman, S.: Spectral discrimination of coarse and fine mode optical depth, J. Geophys. Res., 108, 4559, doi:10.1029/2002JD002975, 2003.

Remer, L. A., Tanré, D., Kaufman, Y. J., Ichoku, C., Mattoo, S., Levy, R., Chu, D. A., Holben, B., Dubovik, O., Smirnov, A., Martins, J. V., Li, R. R., and Ahmad, Z.: Validation of MODIS aerosol retrieval over ocean, Geophys. Res. Lett., 29, 8008, doi:10.1029/2001GL013204, 2002.

Remer, L. A., Kaufman, Y. J., Tanré, D., Mattoo, S., Chu, D. A., Martins, J. V., Li, R. R., Ichoku, C., Levy, R. C., Kleidman, R. G., Eck, T. F., Vermote, E., and Holben, B. N.: The MODIS aerosol algorithm, products, and validation, J. Atmos. Sci., 62, 947–973, doi:10.1175/JAS3385.1, 2005.

Riihimaki, L. D., Vignola, F. E., and Long, C. N.: Analyzing the contribution of aerosols to an observed increase in direct normal irradiance in Oregon, J. Geophys. Res., 114, D00D02, doi:10.1029/2008JD010970, 2009.

Schuster, G. L., Dubovik, O., and Holben, B. N.: Ångström exponent and bimodal aerosol size distributions, J. Geophys. Res., 111, D07207, doi:10.1029/2005JD006328, 2006.

Schwartz, J. and Neas, L. M.: Fine particles are more strongly associated than coarse particles with acute respiratory health effects in schoolchildren, Epidemiology, 11, 6–10, 2000.

Smith, S. J., van Aardenne, J., Klimont, Z., Andres, R. J., Volke, A., and Delgado Arias, S.: Anthropogenic sulfur dioxide emissions: 1850–2005, Atmos. Chem. Phys., 11, 1101–1116, doi:10.5194/acp-11-1101-2011, 2011.

Stanhill, G. and Cohen, S.: Global dimming: a review of the evidence for a widespread and significant reduction in global radiation with discussion of its probable causes and possible agricultural consequences, Agr. Forest Meteorol., 107, 255–278, 2001.

Stanhill, G. and Moreshet, S.: Global radiation climate changes: the world network, Climatic Change, 21, 57–75, 1992.

Streets, D. G., Yan, F., Chin, M., Diehl, T., Mahowald, N., Schultz, M., Wild, M., Wu, Y., and Yu, C.: Anthropogenic and natural contributions to regional trends in aerosol optical depth, 1980–2006, J. Geophys. Res., 114, D00D18, doi:10.1029/2008JD011624, 2009.

Title Page

Abstract | Introduction

Conclusions | References

Tables | Figures

◀ | ▶

◀ | ▶

Back | Close

Full Screen / Esc

Printer-friendly Version

Interactive Discussion

Tanré, D., Kaufman, Y. J., Holben, B. N., Chatenet, B., Karnieli, A., Lavenu, F., Blarel, L., Dubovik, O., Remer, L. A., and Smirnov, A.: Climatology of dust aerosol size distribution and optical properties derived from remotely sensed data in the solar spectrum, J. Geophys. Res., 106, 18205–18217, doi:10.1029/2000JD900663, 2001.

5 Wåhlin, P.: Measured reduction of kerbside ultrafine particle number concentrations in Copenhagen, Atmos. Environ., 43, 3645–3647, doi:10.1016/j.atmosenv.2009.04.023, 2009.

Wang, Y., Hopke, P. K., Chalupa, D. C., and Utell, M. J.: Long-term study of urban ultrafine particles and other pollutants, Atmos. Environ., 45, 7672–7680, doi:10.1016/j.atmosenv.2010.08.022, 2011.

10 Wild, M., Gilgen, H., Roesch, A., Ohmura, A., Long, C. N., Dutton, E. G., Forgan, B., Kallis, A., Russak, V., and Tsvetkov, A.: From dimming to brightening: decadal changes in solar radiation at Earth's surface, Science, 308, 847–850, doi:10.1126/science.1103215, 2005.

Wild, M., Trüssel, B., Ohmura, A., Long, C. N., König-Langlo, G., Dutton, E. G., and Tsvetkov, A.: Global dimming and brightening: an update beyond 2000, J. Geophys. Res., 114, D00D13,

15 doi:10.1029/2008JD011382, 2009.

Title Page

Abstract | Introduction

Conclusions | References

Tables | Figures

◄ | ►

◄ | ►

Back | Close

Full Screen / Esc

Printer-friendly Version

Interactive Discussion

Table 1. Summary of the acronyms.

AOD	Aerosol optical depth (for all particles)
sAOD	Aerosol optical depth for small particles
mAOD	Aerosol optical depth for medium-size particles
lAOD	Aerosol optical depth for large particles
AAOD	Absorption aerosol optical depth; $= (1 - SSA) \times AOD$
SSA	Single scattering albedo
AE	Ångström exponent for AOD
FMF	Fine mode fraction; $= sAOD/AOD$

Table 2. Datasets used in this study.

Measurement	Time period	Data version	Spatial resolution	Wavelength (in nm)
AERONET	Jan 2001–Dec 2010	Monthly level-2		440, 675, 870 500 (AOD and fine-mode fraction)
MODIS/Terra	Jan 2001–Dec 2010	Monthly level-3	$1° \times 1°$	470, 550, 660, 870
MODIS/Aqua	Jul 2002–Dec 2010	Monthly level-3	$1° \times 1°$	470, 550, 660, 870
MISR/Terra	Jan 2001–Dec 2010	Monthly level-3	$0.5° \times 0.5°$	443, 555, 670, 865

Table 3. Definitions of sAOD, mAOD and IAOD. See Table 1 for the AOD acronyms. Only the MISR algorithm gives mAOD.

Measurement	Parameter	Particle size definition (r_p = particle ratius)
AERONET	sAOD	$r_p < 0.6\,\mu m$
	IAOD	$0.6\,\mu m < r_p$
MODIS	sAOD	$r_p \leq 0.5\,\mu m$
	IAOD	$0.5\,\mu m < r_p$
MISR	sAOD	$r_p < 0.35\,\mu m$
	mAOD	$0.35\,\mu m \leq r_p \leq 0.7\,\mu m$
	IAOD	$0.7\,\mu m < r_p$

Observationally-constrained estimates of global small-mode AOD

K. Lee and C. E. Chung

Table 4. Trend from 2001 to 2010 in units of optical depth change over the 10 yr, **(a)** using our best estimate; and **(b)** only using AERONET data. Linear trend is obtained from annual-mean values for each grid, and then average averages are made. "Eastern China" below refers to the 140–132° E/24–52° N portion of China mainland, and "Western Europe" ("US/Canada") the land part of the Western Europe sector (US/Canada sector) in Fig. 1.

(a)	Area-averaged trend		
	AOD (500 nm)	sAOD (500 nm)	AAOD (550 nm)
India + eastern China	−0.028 (−6 %)	0.14 (43 %)	−0.0074 (−17 %)
Western Europe + US/Canada	−0.025 (−20 %)	−0.017 (−20 %)	−0.00036 (−7 %)
Global	−0.0076 (−5 %)	−0.0048 (−5 %)	−0.00034 (−4 %)
(b)	Area-averaged trend		
	AOD (500 nm)	sAOD (500 nm)	AAOD (550 nm)
India + eastern China	−0.0081 (−1 %)	0.047 (16 %)	−0.0047 (−10 %)
Western Europe + US/Canada	−0.035 (−27 %)	−0.032 (−34 %)	−0.0010 (−9 %)
Global	0.026 (12 %)	0.014 (11 %)	0.0019 (9 %)
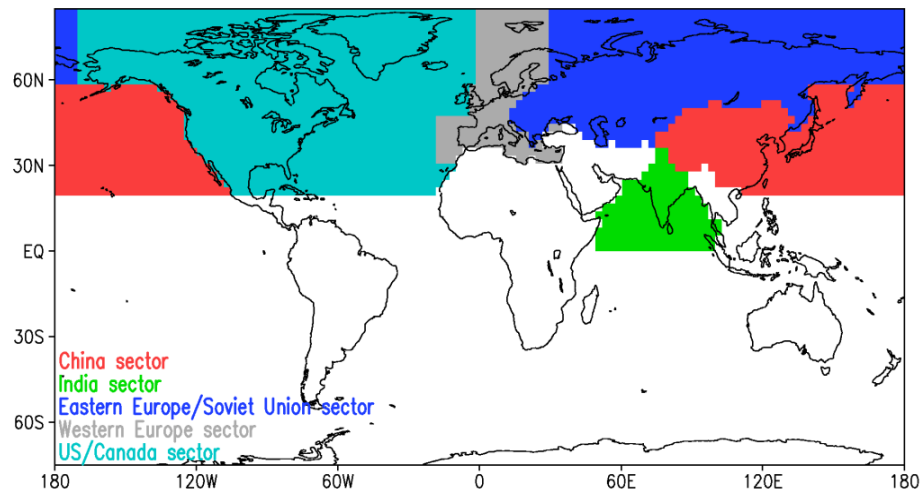
Fig. 1. Division of the world in this study.

China sector
India sector
Eastern Europe/Soviet Union sector
Western Europe sector
US/Canada sector
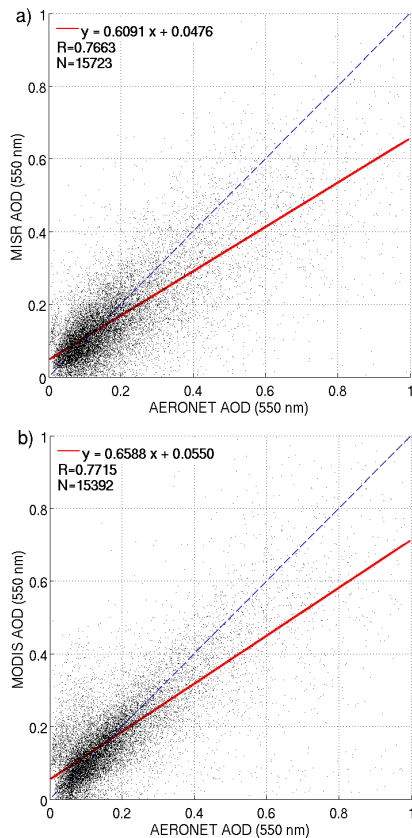
Fig. 2. (a) Comparison of monthly AERONET aerosol optical depths (AODs) and monthly MISR AODs collocated in time and space. **(b)** Comparison with MODIS AODs. Data in the 2001–2010 period is used here. The solid red line in each panel represents the linear regression, and the dashed blue line shows a slope of 1.0. R denotes the correlation coefficient, and N the number of the collocated data.

Title Page

Abstract | Introduction

Conclusions | References

Tables | Figures

◄ | ►

◄ | ►

Back | Close

Full Screen / Esc

Printer-friendly Version

Interactive Discussion
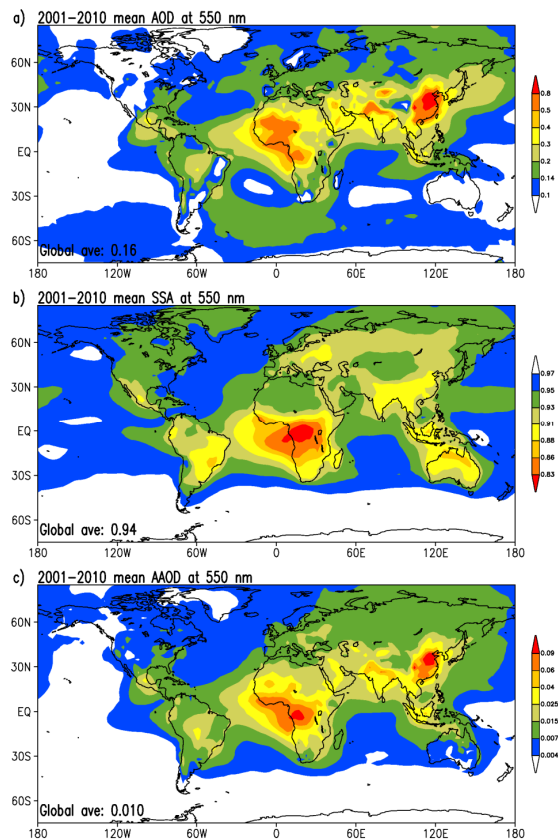
Fig. 3. Our best estimates of aerosol optical properties: AOD by integrating AERONET, MISR, MODIS, and GOCART data; **(b)** single scattering albedo (SSA) by integrating AERONET SSA and GOCART SSA; and **(c)** absorption AOD (AAOD) from the integrated AOD **(a)** and SSA **(b)**. The global and decadal average of SSA in **(b)** is an AOD weighted average.
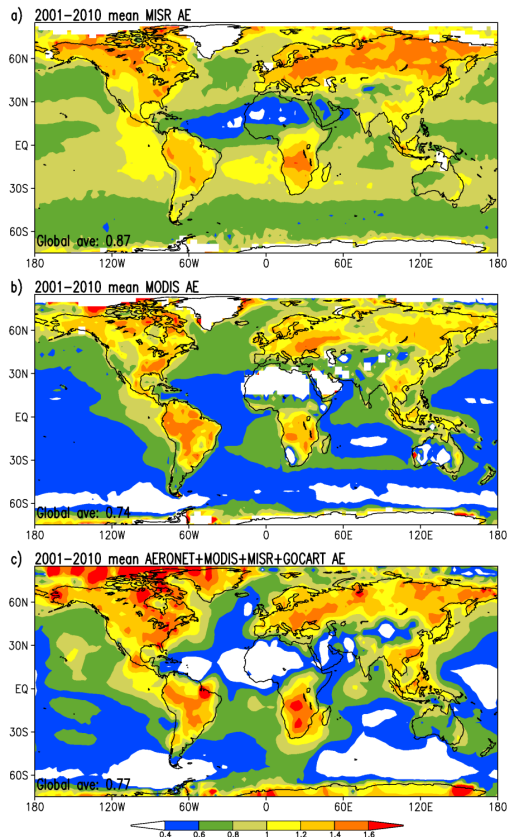
Fig. 4. Ångström exponent (AE) from **(a)** MISR, **(b)** MODIS, and **(c)** our best estimate. Shown are the 10-yr (2001–2010) AE averages, using the 10-yr mean AOD at each wavelength.
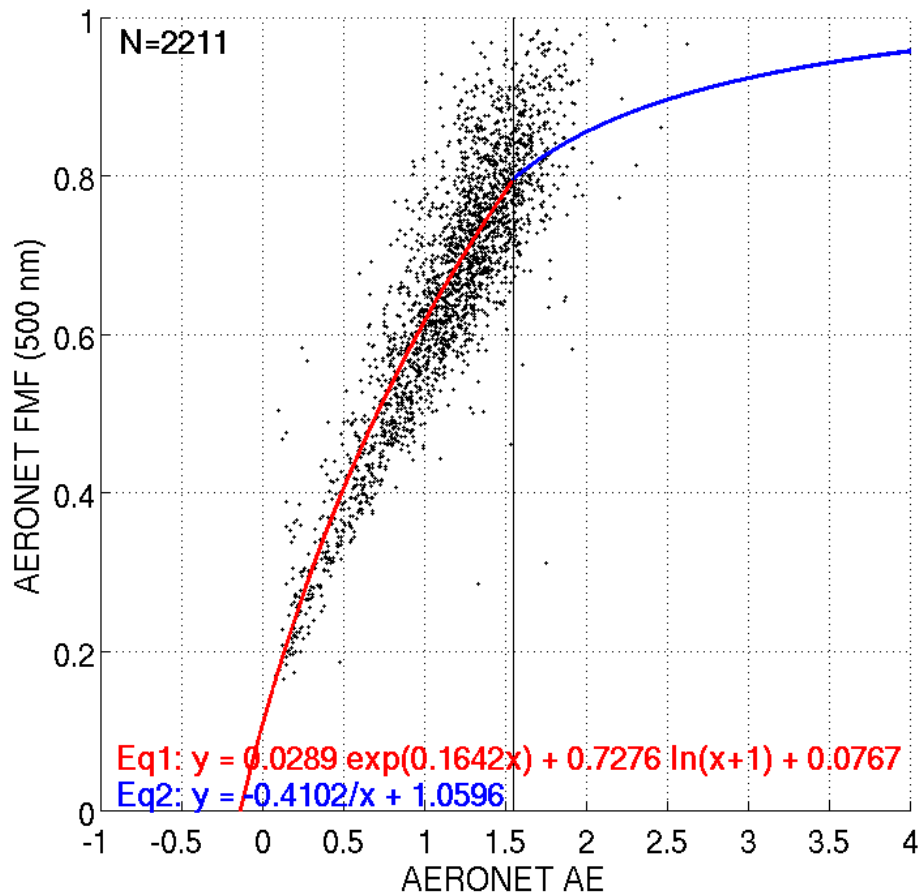
Fig. 5. Comparing monthly AERONET fine mode fraction (FMF) at 500 nm to monthly AERONET Ångström exponent (AE). The red and blue lines represent our best-fit. The fitting equations (Eqs. 1 and 2) and the number of data points (*N*) are given in the plot.

Title Page

Abstract | Introduction

Conclusions | References

Tables | Figures

|◄ | ►|

◄ | ►

Back | Close

Full Screen / Esc

Printer-friendly Version

Interactive Discussion
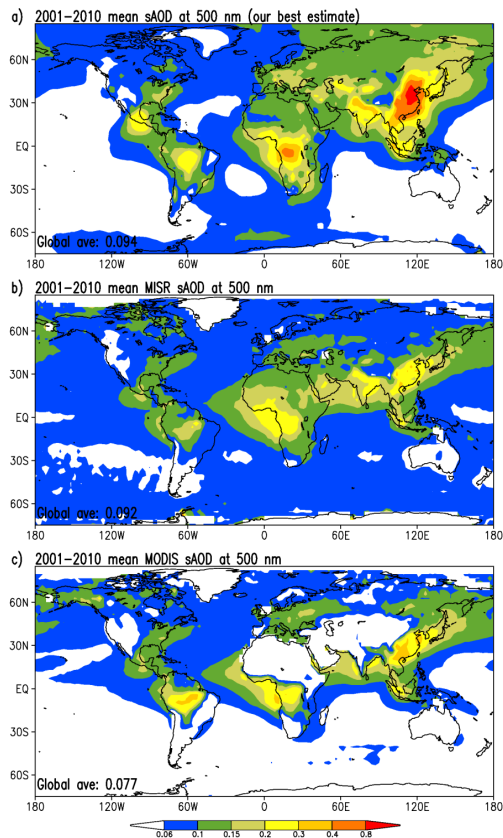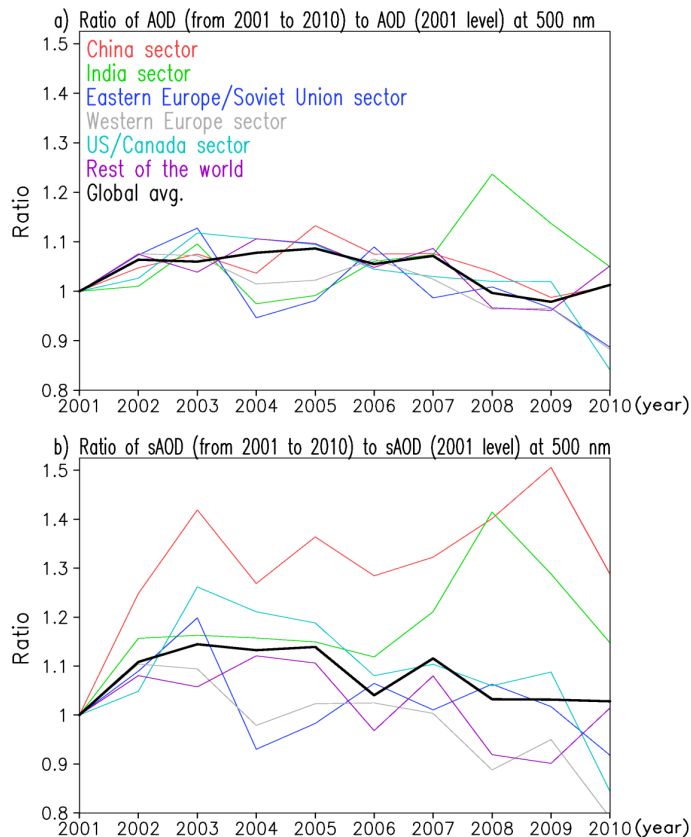
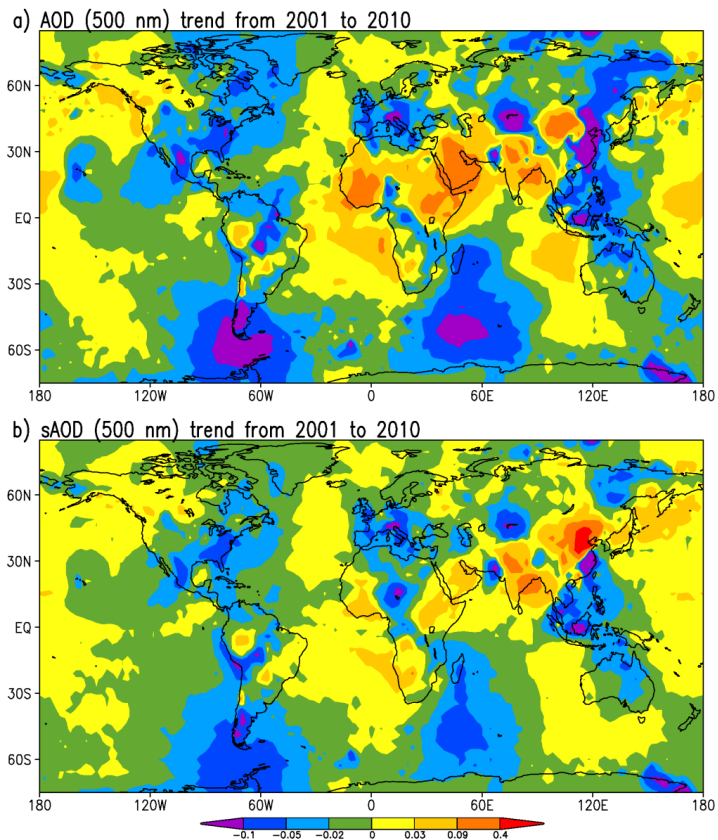**Fig. 6.** Small-mode AOD (sAOD) estimated by: **(a)** our empirical method with the fitting equations as in Fig. 5; **(b)** MISR sAOD; and **(c)** MODIS sAOD.

Fig. 7. Ratio of regionally averaged annual-mean AOD (or sAOD) to its 2001 level. Here, we use our best estimates of AOD (sAOD). See Fig. 1 for the division of the world.

Title Page

Abstract | Introduction

Conclusions | References

Tables | Figures

|◄ | ►|

◄ | ►

Back | Close

Full Screen / Esc

Printer-friendly Version

Interactive Discussion

Fig. 8. Trend from 2001 to 2010 in units of the change over the 10 yr. The trend is computed from annual means for each grid.

Title Page

Abstract | Introduction

Conclusions | References

Tables | Figures

Back | Close

Full Screen / Esc

Printer-friendly Version

Interactive Discussion